A New Methodology to Study the Pantograph-Catenary Dynamics in Curved Railway Tracks

Pedro Antunes*[a,b], Jorge Ambrósio[a], João Pombo[a,b,c] and Alan Facchinetti[d]

[a]*IDMEC, Instituto Superior Técnico, Universidade de Lisboa, Lisboa, Portugal*

[b]*Institute of Railway Research, School of Computing and Engineering, University of Huddersfield, UK*

[c]*ISEL, IPL, Lisboa, Portugal*

[d]*Dipartimento di Meccanica, Politecnico di Milano,Milano, Italy*

Corresponding author e-mail: p.antunes@hud.ac.uk

A New Methodology to Study the Pantograph-Catenary Dynamics in Curved Railway Tracks

The pantograph-catenary system is responsible to provide an uninterrupted energy supply to power electric traction railway vehicles. The analysis of the dynamic behaviour of the catenary and pantograph, as well as its interaction, has been object of active research to improve the energy collection quality. This work proposes an approach for the fully three-dimensional dynamic analysis of pantograph-catenary interaction in general railway tracks including curves. Both the catenary model and the trajectory of the pantograph base are defined with respect to the track geometry considering the conventional definition used by the rail industry, i.e., curvature, cross level and vertical position of the track. The pantograph is modelled using a 3D multibody formulation being its base motion constrained to follow the generalized trajectory from the top of a railway vehicle. The finite element method is used to model the catenary. A co-simulation procedure is set to allow for the coupled dynamics of the two systems. In order to demonstrate the methodology, setting up models for curved catenaries, analyse their modelling implications and highlight applicability, realistic case studies of pantograph-catenary interaction in high-speed rail operations are presented and discussed. In the process there are found significant differences on the dynamic response of the catenary in curved and straight tracks.

Keywords: Railway dynamics, 3D Pantograph-Catenary interaction, Co-Simulation, Curved tracks, Contact mechanics.

1 Introduction

The modern railway systems rely on the cost-effectiveness and reliability of electrical traction vehicles where the pantograph–catenary interface, represented in Figure 1, ensures the supply of electrical energy to power the vehicles motors. Thus, it is not only of fundamental importance that this energy supply remains uninterrupted, but also that its electro-mechanical wear is as reduced as possible.

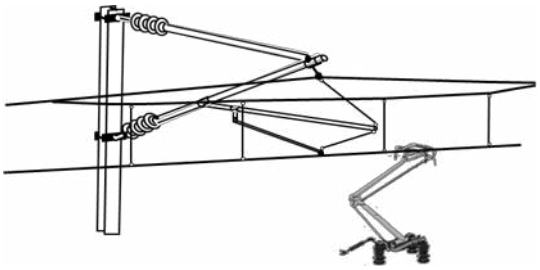

Figure 1: Railway energy collecting system composed of a catenary and a pantograph.

The over-head contact line, also known simply as catenary, is composed of a set of suspended cable wires and its supporting elements that run along the railway track and carry the electrical current, which in turn is collected by the pantograph mounted on the top of the railway vehicle. The energy collection is assured by the sliding contact between the pantograph and the catenary contact wire. The interaction contact force developed must fulfil tight operational requirements that ensure that a reliable and efficient energy collection is achieved. Operating the pantograph-catenary interface at a low average contact force increases the susceptibility to contact loss incidents with consequent arcing, which in turn leads to high electro-mechanical wear and the deterioration of the functional conditions of both the catenary and the pantograph. High contact forces, in the other hand, results in mechanical wear of the contact elements increasing the frequency of the maintenance cycles and risk of failure [1]. Certainly, the present need to increase the rail network capacity and its interoperability puts extra demands on these systems, [2,3], for which the energy collection ability remains a limiting factor of the current railway vehicles operational speeds [4,5].

The dynamic analysis of the pantograph and catenary, as well as their interaction, is object of active research. The development of specialized numerical applications for the dynamic analysis of pantograph-catenary interaction plays a significant role in the analysis and design of railway network assets. An extensive amount of publications on the development and application of computational methods and applications in pantograph-interaction can be found in the literature, addressing analysis of multiple pantograph operation [6–8], analysis of critical catenary sections [9–11], and optimisation of pantograph and catenary designs [12–14] among other issues of importance. The perturbation of the quality of contact in the pantograph-catenary interface due to aerodynamics effects, vehicle vibration and catenary irregularities [15–19] are also considered in the literature. The hardware-in-the-loop hybrid simulations of pantograph-catenary interaction is also another approach to find improved dynamic performance for the two systems [20,21]. Also, research on the identification and influence of catenary

damping, shown as very important for the interaction quality [22], was performed to improve catenary models [23]. The pantograph-catenary benchmarks, [24,25], and its associated references portrait the state-of-the-art of existing numerical analysis tools, developed by world leading research institutions. Notice that in all applications, methods or case-studies considered in previous publications on the topic of pantograph-catenary interaction modelling and analysis, most catenary models are exclusively set in straight railway tracks. The work by Teichelmann et al. [26] presents an application with a curved catenary, but the method on how to build the model is not presented. The employment of catenary geometries consistent with general track geometries, i.e., catenaries with curvatures, is addressed in PantoCat statement of method [27], however this capability is not fully demonstrated. In [28], M. Tur et al. present a methodology for computing the initial configuration of a railway catenary, including catenaries in curved tracks. Also, A. Rønnquist et al. [29] present a modal analysis of catenaries set in general paths and P. Nåvik et al. [30] present the first results obtained from numerical simulations in comparison with field measurements. However, a detailed methodology for the construction of catenary models set in general track trajectories, its modelling implications and the interaction with the pantographs are not addressed in any of the previous works [26–30].

The work presented here purposes an approach for the numerical dynamic analysis of pantograph-catenary interaction in curved tracks or for that matter in any generalized track trajectory. Here both the catenary model and the trajectory path of the pantograph are consistent with the general geometry, which is defined as parametric curve with an associated local reference frame that defines the orientation of the track layout. The track geometry is obtained using the standard information required for railway vehicle dynamics applications, i.e., curvature, cross level and vertical profile as function of the track length. The finite element method is used to model and evaluate the dynamic behaviour of a catenary system following the methodology presented in previous works [31]. To cope with the general geometry of the track and the path of its base, the pantograph model is developed using a spatial multibody dynamics formulation [32]. The pantograph base motion, which is fixed to the railway vehicle roof, is defined by a prescribed kinematic motion constraint [33,34]. As both pantograph and catenary use different formulations, their interaction is established through a co-simulation procedure where a penalty method is used to evaluate the contact force between the pantograph and the catenary [35]. To demonstrate the proposed procedure, a detailed analysis of a

pantograph-catenary interaction is presented in this work for catenary models inserted in tracks with a general geometry, including different curve radii.

2 Track Spatial Definition

The catenary layout is defined in relation to the track travel length, or track arc-length, and its running surface. To define a catenary system in space and to place it correctly in relation to the track, a spatial reference is required. For a catenary on a straight track this process is straight forward. However, when dealing with a generalised track trajectory a more systematic approach is required to account for the track curvature and cross level, which influence the orientation of the running surface of the track. Also, the trajectory of the pantograph is defined by the position of the vehicle roof top relative to the track surface, which enforces that a common geometric framework is used for both systems. The track geometric description commonly used in railway vehicle dynamics studies, is also used here as such a common framework.

The railway track geometry is described as a function of its travel length, by the curvature, cross level and elevation [36]. Though this description defines the track geometry along its travel length, it does not provide an absolute spatial frame with respect to which position other systems. To fulfil this need, a reference moving frame of the track is established as a function of the travel length [37,38]. For a given travelled length *s*, the position of the moving frame origin $\mathbf{r}_t$ is set such way that ξ_t is tangent to the track centreline, η_t is transversal to the track and tangent to the running surfaces of the rails while ζ_t is normal to the track running surface, as shown in Figure 2.

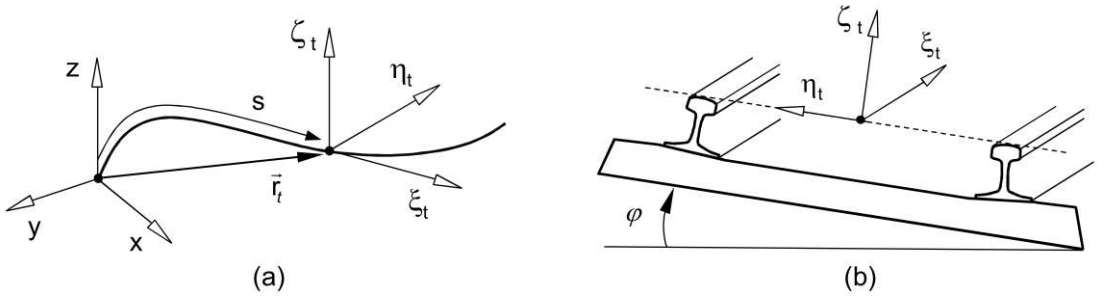

Figure 2: Representation of the track moving frame: (a) As a parametric curve relative to the track length; (b) In relation to the track running surface.

The track centreline spatial curve is obtained by performing the geometric reconstruction of the track geometry using the curvature and elevation data of the selected track [39], which is the same data that is used by the rail industry to represent the track

design. With the track centreline curve and the track cross level and corresponding cant angle, φ, a local moving frame of reference is built along the track using a methodology based on the evaluation and rotation of Frenet-Serret frame, [34,40]. For the purpose of computational applications, the track centreline curve and the moving frame unit vectors, ξ_t, η_t and ζ_t, are discretized in particular locations, such way that, by interpolation, the complete track geometry can be used

3 Catenary Model

The catenary system is modelled in this work using a finite element formulation [41]. The geometric description of the catenary, which is defined in relation to the track running surface, is the basis of the construction of the finite element model used here. Therefore, the catenary layout along the track and its geometric spatial description are presented first. Afterwards, the equations of motion for the finite element model are detailed along with the catenary initialization procedure, i.e., the methodology that allows positioning the finite element mesh nodes in such a way that the catenary is in static equilibrium when the dynamic analysis starts.

3.1 Catenary Layout

A typical catenary structure is composed by two main suspended cable wires, the contact wire and the messenger wire, which are set in tension along the track by mechanical tensioning devices mounted at the end poles of each catenary section. Due to physical and operational reasons, each section has a limited length. Hence the continuity of the contact wire, as seen by the pantograph contact strip, is assured by overlapping catenary sections at its ends. Both the contact and messenger wires are periodically supported by cantilevered consoles, known as cantilevers, mounted in poles, as represented in Figure 3. In between each pole, the contact wire is supported, in a discrete manner, by dropper cables that hang from the messenger wire. Besides supporting the contact wire, the droppers are responsible to minimize its sag and to keep its vertical elasticity as uniform as possible along its span.

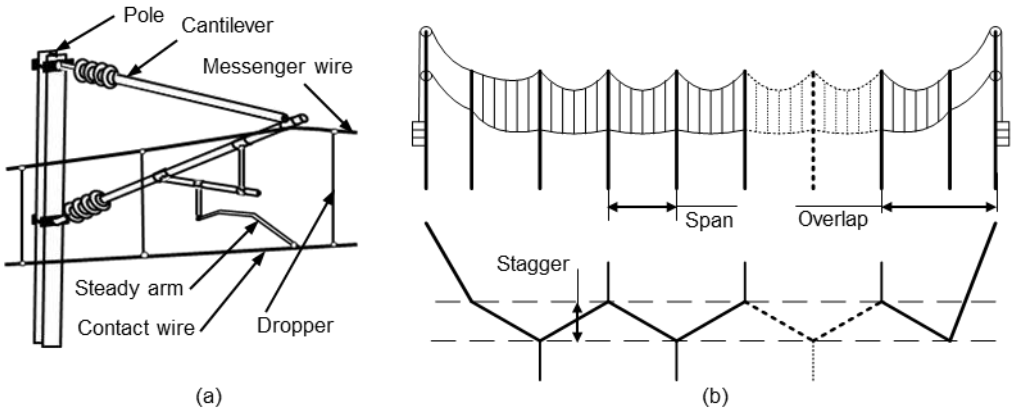

Figure 3: Catenary structure and its main components: (a) Cantilever; (b) Longitudinal and top view.

To avoid grooving and ensure, as much as possible, a uniform wear of the pantograph contact strip, an alternating lateral offset of the contact wire, commonly known as stagger, is imposed at each cantilever. The stagger of the contact wire is provided by a steady arm, which is fixed on the cantilever by a pin joint and designed to allow the vertical movement of the contact wire to provide clearance for the pantograph passage. To provide clearance for the pantograph passage and to allow vertical movement of the contact wire, its supporting connection to the cantilever is achieved by a steady arm, which is fixed on the cantilever by a pin joint. The offset is set in relation to the nominal trajectory of the pantograph contact strip, which in straight tracks is just a straight line located at a given height above track centreline. Generally, the offsets are determined in order to keep the span lengths as long as possible, to reduce construction costs, while still ensuring that the contact wire deflection, under wind conditions, never exceeds a permissible lateral displacement, e_{perm}, such that the contact wire is always within the usable length of the contact strip [42]. In straight lines and very large radius curves this results in an alternating offset pattern *(±b)*, or *zig-zag*, as represented in Figure 4 (a). Note that the lateral forces, $\mathbf{f}_{sp}$, at the contact wire supports, which result from the imposed change of direction of the tensioned contact wire, have defined maximum and minimum tolerances [43]. Also, a minimum lateral sweep of the contact wire must be ensured to avoid grooving. As a result of these constraints, as the track curvature increases, a reduction of the offset at the inner side of the curve is required, thus forcing $b_1 \neq b_2$, as shown in Figure 4 (c).

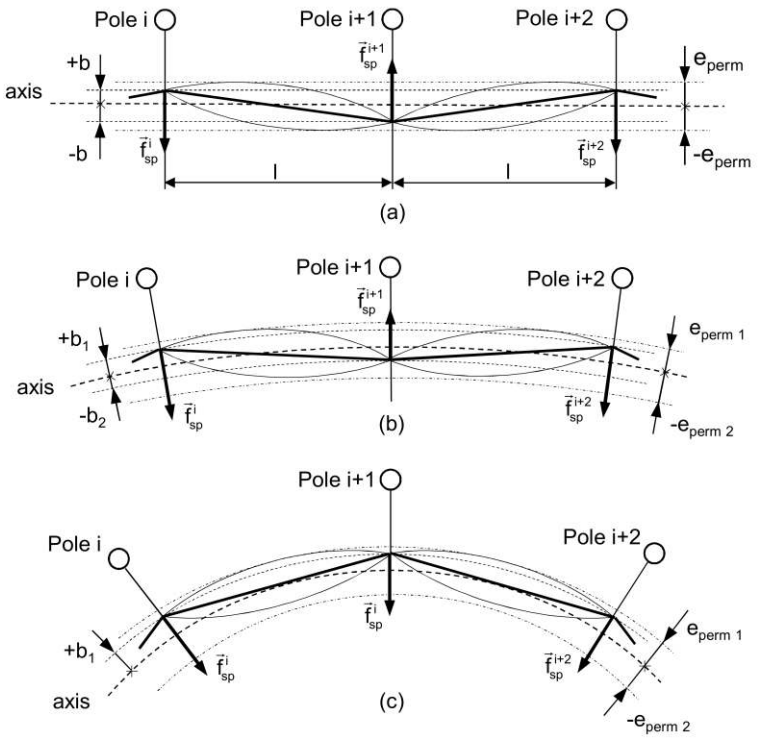

Figure 4: Contact wire lateral position on: (a) Straight track, (b) Large radius curves; (c) Small radius curves.

For small radius curves the offset is placed always on the outside side of the curve, i.e., $(+b_1,+b_1)$. Eventually, for even smaller radius it is not possible to use suitable offsets while maintaining the span length and shorter spans need to be used. Moreover, note that direction of the lateral forces at the steady arm support result from the imposed stagger and can either act away or towards the pole which determine the position and orientation of the steady arm in a pull-off or push-off configuration.

When designing a catenary system, the positioning of the offsets along each cantilever must take into consideration the catenary design, specified operational requirements set by the infrastructure owners and by standards [44]. This results in a set of catenary layout rules that define the allowed span lengths and correspondent staggering for defined ranges of track curvature, which can be specific to a given wind region. The determination of these design rules can follow different approaches being its detailed discussion beyond the scope of this work [45]. For catenary systems belonging to different railway networks in current operation, Table 1 presents a summary of the maximum allowed span lengths, l_{max}, and correspondent stagger, (b_1,b_2), set for different track curvatures, on a given wind region. Due to confidentiality, the railway network remains unidentified.

Catenary	A			B			C		
Operating Speed [km/h]	160			200			300		
Curve Radius [m]	l_{max} [m]	b_1 [mm]	b_2 [mm]	l_{max} [m]	b_1 [mm]	b_2 [mm]	l_{max} [m]	b_1 [mm]	b_2 [mm]
∞	80	+400	-400	63	+200	-200	65	+300	-300
10000	80	+400	-300	63	+200	-200	65	+300	-190
7000	76	+400	-330	63	+240	-50	65	+300	-150
5000	76	+400	+120	63	+240	-50	65	+300	-90
4000	80	+400	+150	63	+240	0	65	+300	-40
3000	80	+400	+310	63	+240	+90	65	+300	+50
2000	80	+400	+400	63	+240	+240	65	+300	+230
1000	67	+400	+400	54	+240	+240	63	+300	+300

Table 1: Catenary span length and stagger set in relation to the track curvature in different catenary systems.

Note that there are different catenary designs [31,43], with slightly different or more accentuated topological arrangements such as the stich-wire and compound catenaries. However, simple alternatives are more extensively used. For the sake of simplicity, the approach proposed here is applied for the setup of catenary models of the simple type. Nevertheless, this methodology can be applied to any type of catenary.

3.2 Catenary Model Geometry

The finite element model of the catenary is defined firstly by setting the geometric positions of the catenary subsystems made by the contact and messenger wire points at the cantilever and at each dropper connection. With reference to Figure 5, at each cantilever, the positions of the contact wire at the steady arm, $\mathbf{r}_{cw}$, and the messenger wire at its cantilever support, $\mathbf{r}_{mw}$, are determined as:

$$\begin{aligned} \mathbf{r}_{cw} &= \mathbf{r}_t + \mathbf{A}_t \mathbf{s}'^{t}_{cw} \\ \mathbf{r}_{mw} &= \mathbf{r}_{cw} + \mathbf{s}^{cw}_{mw} \end{aligned} \tag{1}$$

where $\mathbf{r}_t$ is the position vector of the track centreline and $\mathbf{A}_t$ is the rotation matrix associated to the local reference frame, $(\xi, \eta, \zeta)_t$, which defines the track running surface orientation. These quantities are obtained by the evaluation of the track moving frame, described in Section 2, at the track length in which the pole is mounted. Vectors $\mathbf{s}'^{t}_{cw}$ and $\mathbf{s}^{cw}_{mw}$ are, respectively, the position of the contact wire in respect to the local reference frame $(\xi, \eta, \zeta)_t$ and the position of the messenger wire relation to the contact wire

position, $\mathbf{r}_{cw}$, evaluated as:

$$\begin{aligned} \mathbf{s}_{cw}^{tt} &= \begin{bmatrix} 0 & \pm b & h_{cw} \end{bmatrix}^T \\ \mathbf{s}_{mw}^{cw} &= \begin{bmatrix} 0 & 0 & h_e \end{bmatrix}^T \end{aligned} \tag{2}$$

where the parameters b, h_{cw} and h_e are respectively, the contact wire lateral offset relative to the track centreline, the nominal contact wire height relative to the running surface and the encumbrance of the cantilever which sets the distance between the contact and messenger wire.

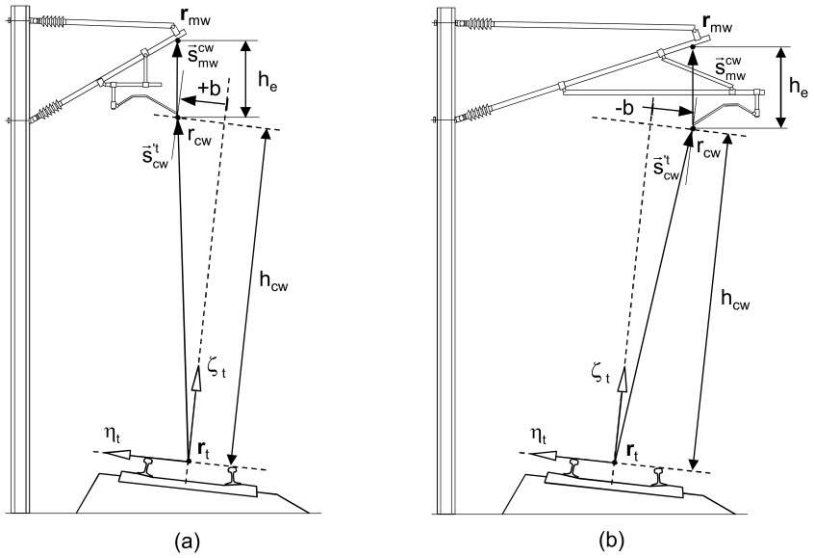

Figure 5: Representation of the contact and messenger wire position on the cantilever, in a curved track: (a) pull-off configuration; (b) push-off configuration.

At each span, the position of the contact and messenger wires at the dropper connections is defined by the dropper spacings, a_d, the dropper lengths, l_d, and the appointed contact wire pre-sag set at for each dropper, s_d. In practice these parameters are set in pre-calculated span tables for a collection of normalised span lengths, l_{span}, of a particular catenary design, as represented in Figure 6. By superimposing these span geometry parameters with the already determined contact and messenger wire position at the cantilever, $\mathbf{r}_{cw}$ and $\mathbf{r}_{mw}$, the position of the contact and messenger wires at each dropper *j,* are defined as:

$$\begin{aligned} \mathbf{d}_{cw}^{j} &= \mathbf{r}_{cw}^{i} + \sum^{j} a_d^j \left(\frac{l_{cw}}{l_{span}} \right) \hat{\mathbf{u}}_{cw} + [0 \quad 0 \quad -s_d^j]^T \\ \mathbf{d}_{mw}^{j} &= \mathbf{d}_{cw}^{j} + [0 \quad 0 \quad l_d^j]^T \end{aligned} \tag{3}$$

where $l_{cw} = \left\| \mathbf{r}_{cw}^{i+1} - \mathbf{r}_{cw}^{i} \right\|$ is the length between the subsequent cantilever contact wire

positions and $\hat{\mathbf{u}}_{cw} = \left(\mathbf{r}_{cw}^{i+1} - \mathbf{r}_{cw}^{i}\right) / l_{cw}$ is the corresponding versor.

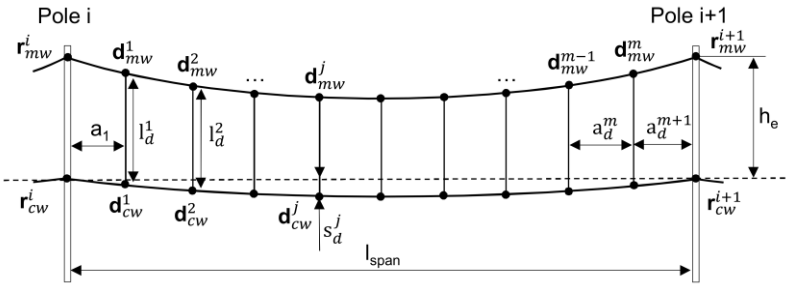

Figure 6: Catenary span geometric parameters.

3.3 Catenary Finite Element Model

The motion of the catenary is characterized by small rotation and small deformations where the only nonlinear effect is the dropper slacking resulting from the pantograph passage. The constant axial tensioning of the contact and messenger wires should also not be neglected. Therefore, the catenary is here modelled with linear finite elements where dropper slacking compensating forces are added, such that the dynamic equilibrium equation is assembled as:

$$\mathbf{M}\mathbf{a}_{t+\Delta t} + \mathbf{C}\mathbf{v}_{t+\Delta t} + \mathbf{K}\mathbf{d}_{t+\Delta t} = \mathbf{f}_{t+\Delta t} \tag{4}$$

where **M**, **C** and **K** are the catenary finite element global mass, damping and stiffness matrices. At time $t+\Delta t$, the accelerations, velocities and displacements vector are represented respectively as **a**, **v** and **d** while the sum of all external applied forces is depicted by vector **f**. All catenary elements are modelled using two-node Euler–Bernoulli beam elements [41], with the exception of the messenger wire cantilever support which is modelled as an equivalent three dimensional spring-damper element. The mass of the clamps and claws, present on the catenary structure to join its components, are modelled as lumped masses. To represent the stress stiffening of the catenary structure due to the tension stress state caused by tensioning the cable wires the stiffness matrix of the beam element *i* used for the contact and messenger wire is evaluated as:

$$\mathbf{K}_i^e = \mathbf{K}_L^e + F\,\mathbf{K}_G^e \tag{5}$$

in which $\mathbf{K}_L^e$ is the linear Euler-Bernoulli beam element stiffness matrix, F is the axial tension and $\mathbf{K}_G^e$ is the element geometric matrix. Proportional damping, also known as Rayleigh damping [46], is used to evaluate each beam finite element damping matrix $\mathbf{C}^e$ such that:

$$\mathbf{C}^e = \alpha^e \mathbf{M}^e + \beta^e \mathbf{K}^e \tag{6}$$

being α^e and β^e the mass and stiffness proportionality factors set for each type of catenary component. Alternatively, the same proportionality factors α and β are used for all structural elements. For a time, t+Δt the force vector $\mathbf{f}_{t+\Delta t}$ is evaluated as:

$$\mathbf{f}_{t+\Delta t} = \mathbf{f}^g + \mathbf{f}^t + \mathbf{f}^c_{t+\Delta t} + \mathbf{f}^d_{t+\Delta t} \tag{7}$$

where vector $\mathbf{f}^g$ contains the gravitational forces and $\mathbf{f}^t$ is made of the forces responsible for tensioning the wires individually applied at each tensioned element as pre-stress. Vector $\mathbf{f}^c_{t+\Delta t}$ and $\mathbf{f}^d_{t+\Delta t}$ are evaluated each time $t+\Delta t$ and represent the equivalent contact forces and moments applied at the appropriate nodes of the contact wire element and the dropper slacking compensating forces evaluated as:

$$\mathbf{f}^d_{t+\Delta t} = \sum_i \left(\mathbf{B}_d \mathbf{K}^e_d \tilde{\mathbf{d}}^e_{t+\Delta t} \right)_i \tag{8}$$

where for any dropper i that is slack, $\mathbf{K}^e_d$ is its stiffness matrix and $\tilde{\mathbf{d}}^e_{t+\Delta t}$ is a close prediction of its nodal displacements. The Boolean matrix $\mathbf{B}_d$ simply maps the local coordinates of the dropper element into the global nodal coordinates of the model. At each evaluated time $t+\Delta t$, the dropper slacking compensating forces are evaluated iteratively with equation (4) until convergence is reached, such that $\left| \mathbf{d}_{t+\Delta t} - \tilde{\mathbf{d}}_{t+\Delta t} \right| < \varepsilon_d$. Here, ε_d is a defined tolerance and vector $\mathbf{d}_{t+\Delta t}$ denotes the displacement vector of the last iterative evaluation of equation (4). Vector $\tilde{\mathbf{d}}_{t+\Delta t}$ refers to the predicted nodal displacements that are either taken from the previous iteration or , in case of being the first iteration, correspond to the previous time step solution. The finite element mesh of the catenary is constructed following closely the catenary geometry established in Section 3.2, one beam element is used for each dropper and steady arm and, at least, 6 elements between droppers are used to define the contact and messenger wires. The model is constrained by pinned points at the ends of the contact and messenger wires, at the steady arm on the cantilever side and at the end of the cantilever messenger wire support.

3.4 Catenary Finite Element Model Initialization

The catenary initialization corresponds to the procedure set to determine the undeformed mesh of the model that upon being statically loaded by the gravitational and axial tension loads exhibit a correct static deformed shape, with special attention to the contact wire

position along the track and its sag. In reality, a similar problem exits when mounting a catenary system on track where, after the first mounting stage, the catenary must be adjusted to fit all geometric specifications. These adjustments are generally comprised on regulating the dropper lengths and the steady arm position at the cantilever. In analogy to this procedure the catenary initialization is formulated here as a minimisation problem, to be solved using a classical gradient based optimisation procedure [47]. Here the minimization problem is defined as:

$$\begin{aligned} &\min\left(\sum_{1}^{m}\left\|\mathbf{d}_{cw}^{S\,\mathrm{m}}(\mathbf{x})-\mathbf{d}_{cw}^{\mathrm{m}}\right\|\right) \\ &\text{subject to: } \mathbf{x}=\left[l_0^1, l_0^2, \ \ldots\ , l_0^m\right] \end{aligned} \tag{9}$$

where the initial dropper lengths, l_0, are set as design variables used to construct the catenary model. The evaluation of the fitness function implies the static analysis of the generated finite element mesh. The deviations between the deformed contact wire positions at the droppers, $\mathbf{d}_{cw}^{S}$, and their nominal positions, $\mathbf{d}_{cw}$, are evaluated. The minimisation problem is solved iteratively for each span where also pinned point constraints are added on the contact and messenger wire cantilever supports, as represented in Figure 7 (a). After the minimisation problem being solved, these constraints are released and substituted by pre-stress forces imposed on the messenger wire support element and the steady arm element. At the contact wire support, the solicitation on each constraint is decomposed on a lateral offset force, $\mathbf{f}_{lat}$, that results from the imposed stagger and a vertical force, $\mathbf{f}_z$, resulting from a residual support of the contact wire weight. These forces are not only used to calculate the pre-stress force to be applied on the equivalent steady arm beam element, $\mathbf{f}_{ps}$, but are also used to set its orientation, as represented on Figure 7 (b).

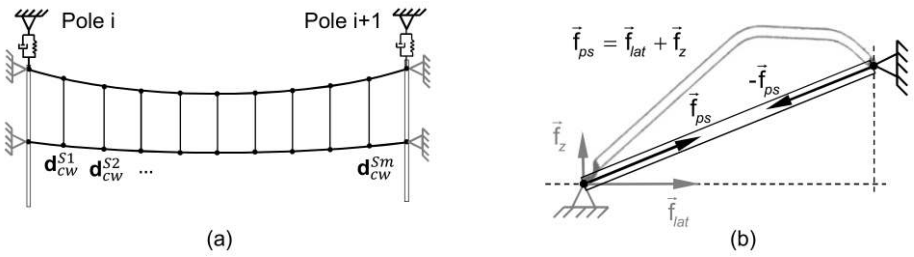

Figure 7: (a) Representation of the deformed catenary span resulting from the solution of the minimisation problem; (b) Representation of the steady-arm pre-stress forces and their orientation.

4 Pantograph Model

A pantograph is a multibody system that can be modelled as such, as seen in Figure 8 (a) or by a lumped mass representation, as observed in in Figure 8 (b). When modelled as a lumped mass, the pantograph model may have 2 masses, as in the case of low or medium train speed operations, or may need to have 3 masses, to account for the upper arm deformability in the case of lighter design as for the case high speed applications. Mechanically, the pantograph unfolding system is such that, during its lifting motion, the head of the pantograph is maintained levelled and its movement is set along a straight line perpendicular to the plane of the pantograph base. In turn, the base is attached to the roof of the railway vehicle, with electric isolators in-between, in perfect alignment with the centre of the vehicle bogie. This is to ensure that, when curving, the centre of pantograph head does not deviate from the centre of the track more than it is to be expected in face of the vehicle dynamics and all allowed clearances and kinematic gauges [48].

Two alternative approaches are generally used to model the pantograph system, the lumped mass model and the multibody model, [17,49]. Each approach has its advantages and drawbacks, being both models suitable to be used in a multibody system dynamics computational environment. The pantograph multibody model assumes the pantograph described by a set of bodies interconnected by force elements and joint constraints representing the structural and mechanical components of the pantograph. Despite of representing properly the pantograph moving elements, the multibody models developed until now are composed of rigid bodies connected by perfect kinematic joints, which do not allow the model to fully describe the realistic behaviour of the pantograph in its complete operating frequency range [50,51]. Due to the scope of this work a multibody representation of the lumped mass model is here adopted. This model consists on a series of lumped masses linked sequentially to a ground by spring/damper elements, as represented in Figure 8 (b). The masses, $m_{1\text{-}3}$, spring, $k_{1\text{-}3}$, and damping, $c_{1\text{-}3}$, coefficients are parameters identified experimentally in laboratory tests [52,53] in order for the model to have the same frequency response of the real pantograph. Thus, these parameters have no direct physical correspondence with the real pantograph with the exception of the upper stage parameters of m_3, k_3, and c_3 which are matched to the mass, stiffness and damping of the collector suspension. For high speed railway applications, there is a minimal requirement of three lumped mass stages to allow for representation of the dynamic behaviour of the system [54]. Regardless of its simple topology the fidelity of the lumped mass pantograph model in representing the dynamic response of a pantograph is recognised, being an industry standard and commonly used by operators, manufacturers

and homologation bodies instead of more complex multibody models. However, note that this work follows the assumption that the dynamic response of the pantograph, identified in laboratory tests, is not affected by the pantograph roll. Although reasonable, as shown in [30], this assumption is to be followed by further research in order to determine the minimal requirements for pantograph models employed in curved tracks.

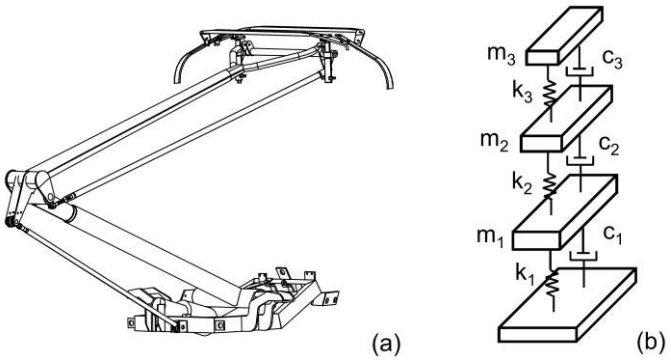

Figure 8: Pantograph models: (a) Multibody; and (b) Lumped mass.

4.1 Multibody Lumped Mass Pantograph Model

A multibody model is characterized by a set of rigid and/or flexible bodies interconnected by force elements and joints that constrain their relative motion. The equations of motion that represent the multibody lumped mass model here considered are written together with the second time derivative of the constraint equations as [32]:

$$\begin{bmatrix} \mathbf{M} & \mathbf{\Phi}_q^T \\ \mathbf{\Phi}_q & \mathbf{0} \end{bmatrix} \begin{Bmatrix} \ddot{\mathbf{q}} \\ \boldsymbol{\lambda} \end{Bmatrix} = \begin{Bmatrix} \mathbf{g} \\ \boldsymbol{\gamma} \end{Bmatrix} \tag{10}$$

where $\ddot{\mathbf{q}}$ is the vector with the accelerations of the rigid bodies $\boldsymbol{\lambda}$ is the Lagrange multiplier vector associated to the joint reaction forces. The remaining terms are described hereafter.

The detailed representation of the multibody lumped mass model considered for this work is depicted in Figure 9. The model is composed by four aligned bodies, $b_{0\text{-}3}$, representing the three staged lumped masses and the pantograph base. Their mass properties, $m_{1\text{-}3}$, are used to form the mass matrix **M** in Equation (10). The spatial position and orientation of the bodies are included in vector **q**, which is evaluated by integrating the accelerations resulting from the solution of Equation (10) during the dynamic analysis of the pantograph. Vector **q** contains, for each body, a set of Cartesian coordinates with the position of its centre of mass and a set of Euler parameters that define its orientation via a local reference frame, $(\xi, \eta, \zeta)_{0-3}$. The linear spring and damper elements placed in

between the masses are formulated as force elements where the forces transmitted to the connected bodies are included in the vector force, **g**. Also included in this vector are the resultant contact force and transport moment, $\mathbf{f}_3^c$ and $\mathbf{n}_3^c$, applied on the lumped mass pantograph top body centre, b_3, and the pantograph static uplift force, $\mathbf{f}_{up}$, applied on the bottom lumped mass body, b_1, which is set to raise the pantograph lumped masses and adjust the resulting average contact force. The kinematic constraints and joints set on the model, along with its respective geometric parameters, are used to form the constraint equations, whose second time derivative includes the Jacobian matrix, $\mathbf{\Phi}_q$, and the right-hand side vector, $\boldsymbol{\gamma}$. In the pantograph lumped mass model, to maintain its unidimensional actuation, three prismatic joints, $pris_{1\text{-}3}$, are set between each lumped mass body and the pantograph base such that the motion of the lumped masses is constrained to be along an axis perpendicular to the plane of the pantograph base as also preventing their relative rotation.

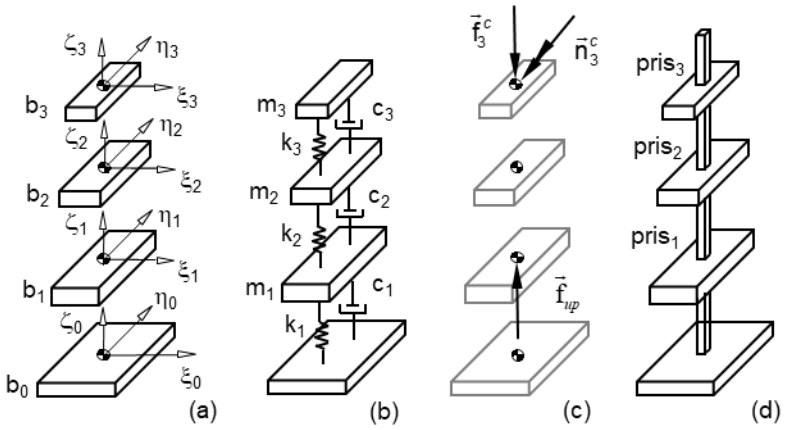

Figure 9: Representation of the multibody lumped mass model: (a) Lumped mass bodies; (b) Spring and damper elements; (c) External applied forces; (d) Prismatic constraints.

To set the trajectory of the pantograph along the track path a prescribed kinematic motion constraint is set to the pantograph base body, b_0, where its position, $\mathbf{r}_0$, and orientation, $(\xi,\eta,\zeta)_0$, is set to follow a moving frame correspondent to the trajectory of the pantograph, as represented in Figure 10. At a given track length, the position, $\mathbf{r}_p$, and local reference frame, $(\xi,\eta,\zeta)_p$, that define the pantograph trajectory are built in relation to the track moving frame, established in Section 1, such that:

$$\begin{aligned} \mathbf{r}_p &= \mathbf{r}_t + \mathbf{A}_t \mathbf{s}_0'^t \\ \boldsymbol{\xi}_p \equiv \boldsymbol{\xi}_t \;\; ; \;\; \boldsymbol{\zeta}_p \equiv \boldsymbol{\zeta}_t \;\; ; \;\; \boldsymbol{\eta}_p &\equiv \boldsymbol{\eta}_t \end{aligned} \tag{11}$$

where $\mathbf{s}_0''$ is the coordinate position of the pantograph base relative to the track local reference frame, $(\xi,\eta,\zeta)_t$, which is defined by the position of the vehicle rooftop, in relation to the track running surface. Matrix $\mathbf{A}_t$ is the rotation matrix associated to track local reference frame $(\xi,\eta,\zeta)_t$.

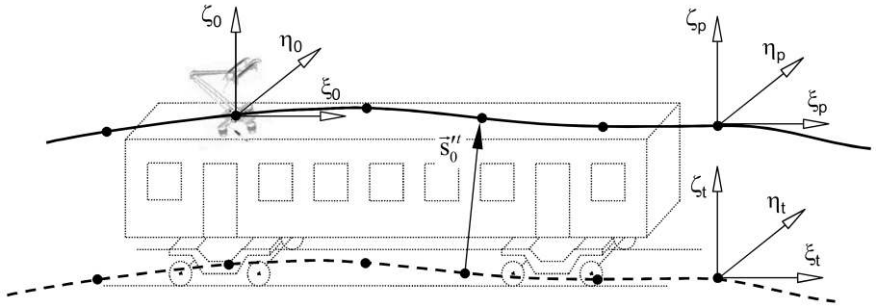

Figure 10: Representation of the prescribed kinematic motion constraint set to the pantograph base.

Note that, in the work presented here, the trajectory of pantograph follows that of the train carbody roof where the pantograph is mounted, which in turn is that of the vehicle that directly follows the track geometry. Using the same methodology, it is possible to include vehicle vibrations by adding them to the pantograph prescribed moving frame. However, it has been shown that track irregularities and car vibrations do not lead to perturbations on the pantograph motion worth accounting for [55].

5 Pantograph-Catenary Interaction

The dynamic analysis of the pantograph-catenary interaction represents a coupled problem in which the dynamic behaviour of the two sub-systems is affected by each other. The classical and most direct methodology to solve this coupling problem is to use the same formulation for both models, such as in the case of pantograph-catenary interaction where the equations of motion of a lumped mass pantograph are added to the finite element equations of the catenary [31]. With the finite element approach described, it is not possible to model the pantograph motion in any other type of operation than its motion in straight track. This is unless additional information to set the pantograph absolute position and orientation in relation to the lumped mass nodal displacements is provided as proposed in [30]. In this work, due to the requirements that each formulation needs to fulfil when dealing with generalized trajectories of the track, a simple formulation is used for each one of the sub-systems, i.e., the finite element method for the catenary and the multibody dynamics formulation for the pantograph. To couple both sub-systems, a co-

simulation environment is setup where the dynamic analysis of each sub-system is done independently [35,56]. Generally, in co-simulation the coupling is either described by imposing a kinematic constraint between the models or by defining a set of constitutive interaction laws [57]. For the pantograph-catenary co-simulation procedure presented here, the latter coupling approach is used, where the constitutive interaction laws lead to contact forces, which in turn result in a set of forces/torques applied on each sub-system. A penalty force methodology is used here to represent the interaction, i.e., to evaluate the contact force between the pantograph and the catenary.

5.1 Pantograph-Catenary Contact Model

From the contact mechanics point of view, the contact between the pantograph contact strip and the catenary contact wire is physically a contact between a flat surface, made of carbon, and a cylinder surface, made of a copper alloy, as represented in Figure 11. Due to the nature of the contact between both types of materials and contact surfaces, the sliding friction forces are neglected, being only the normal contact force, perpendicular to the flat surface of the contact strip considered in this work.

For the penalty formulation used here, the contact force evaluation is dependent on the contact geometry. In this sense, consider the contact geometry presented in Figure 11 where points *a* and *b* represent the extremities of the top surface of the pantograph contact strip. The point positions, $\mathbf{r}_a$ and $\mathbf{r}_b$, are evaluated as:

$$\begin{aligned} \mathbf{r}_a &= \mathbf{r}_3 + \mathbf{A}_3\mathbf{s}'^3_a \quad ; \quad \mathbf{s}'^3_a = \begin{bmatrix} 0 & -l_{cs}/2 & 0 \end{bmatrix}^T \\ \mathbf{r}_b &= \mathbf{r}_3 + \mathbf{A}_3\mathbf{s}'^3_b \quad ; \quad \mathbf{s}'^3_b = \begin{bmatrix} 0 & l_{cs}/2 & 0 \end{bmatrix}^T \end{aligned} \tag{12}$$

where $\mathbf{r}_3$ is the global coordinate position of the lumped mass pantograph top body and $\mathbf{A}_3$ is the rotation matrix associated to its local reference frame $(\xi,\eta,\zeta)_3$. Vector $\mathbf{s}'^3_a$ and $\mathbf{s}'^3_b$ are correspondingly the positions of points *a* and *b* relative to the body local reference frame, evaluated as:

$$\begin{aligned} \mathbf{s}'^3_a &= \begin{bmatrix} 0 & -l_{cs}/2 & 0 \end{bmatrix}^T \\ \mathbf{s}'^3_b &= \begin{bmatrix} 0 & l_{cs}/2 & 0 \end{bmatrix}^T \end{aligned} \tag{13}$$

being l_{cs} the length of the pantograph contact strip.

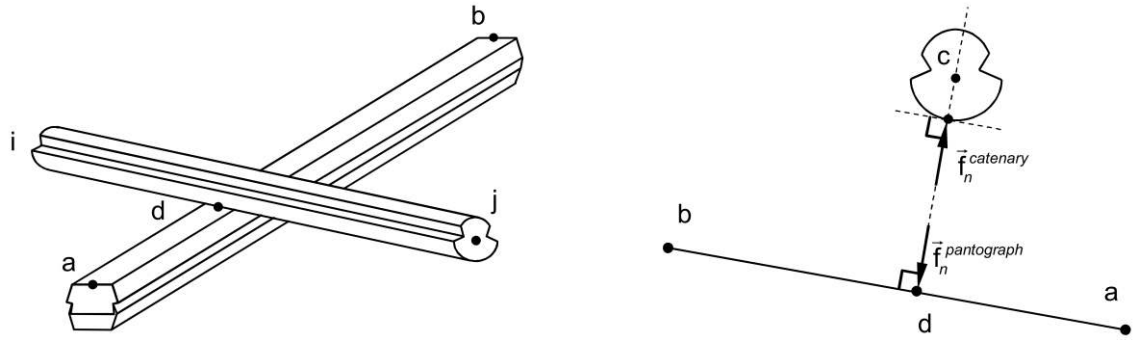

Figure 11: Representation of the pantograph-catenary contact geometry.

Point *c* is the position of the centre of the contact wire cross section, which includes the candidate contact point on the catenary. As the catenary geometry is described in a finite element formulation, point *c* belongs to one of the catenary finite elements that is connected to nodes *i* and *j*, as represented in Figure 12 (a). Therefore, the coordinate position of *c*, $\mathbf{r}_c$, is evaluated as:

$$\begin{aligned} \mathbf{r}_c &= \mathbf{r}_c^0 + \mathbf{N}(\xi)[\mathbf{d}_i \quad \mathbf{d}_j] \\ \mathbf{r}_c^0 &= \mathbf{r}_i^0 + \xi(\mathbf{r}_j^0 - \mathbf{r}_i^0) \end{aligned} \tag{14}$$

where $\mathbf{d}_i$ and $\mathbf{d}_j$ are the node displacements of the contact wire finite element and $\mathbf{r}_c^0$ refers to the corresponding position of *c*, c^0, in the undeformed finite element mesh of the catenary, such that:

$$\mathbf{r}_c^0 = \mathbf{r}_i^0 + \xi(\mathbf{r}_j^0 - \mathbf{r}_i^0) \tag{15}$$

Matrix $\mathbf{N}(\xi)$ contains the beam element shape functions, [58], evaluated at the parametric length coordinate of the finite element, ξ, in which the contact takes place with correspondence to point *c*. The parametric coordinate, ξ, is obtained by finding the intersection between the lines defined by points *a* and b and points i and j, when projected on the same plane. For convenience, as represented in Figure 12 (b), the *xy* plane is used here. The interception between both lines of the contact strip and of the contact wire is expressed as:

$$\mathbf{r}_i^{xy} + \hat{\mathbf{u}}_{ij}^{xy}\lambda_{ic}^{xy} = \mathbf{r}_a^{xy} + \hat{\mathbf{u}}_{ab}^{xy}\lambda_{ac}^{xy} \tag{16}$$

where the superscript *xy* denotes here the projection on the *xy* plane and $\hat{\mathbf{u}}_{mn}$ is the versor of a generic vector that goes from node *m* to node *n*. The scalar values λ_{ic}^{xy} and λ_{ac}^{xy} are the distance between points *i* and *c* and points *a* and *c* in the *xy* plane. These can be obtained by solving equation (16) from which the parametric coordinate ξ can be

evaluated as:

$$\xi = \frac{\lambda_{ic}^{xy}}{\left\| \mathbf{r}_j^{xy} - \mathbf{r}_i^{xy} \right\|} \tag{17}$$

where $\xi \in [0,1]$. If $\xi \notin [0,1]$ the catenary finite element considered does not fit the contact geometry and another element along the contact wire must be tested for contact.

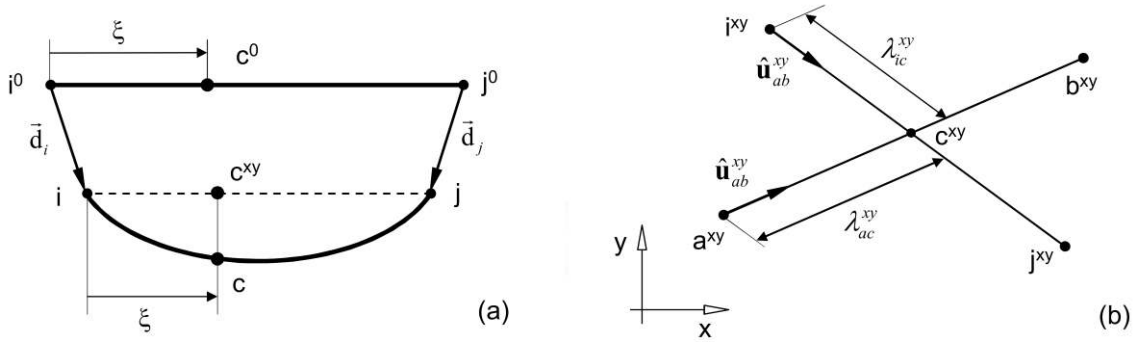

Figure 12: (a) Representation of the contact wire finite element in which contact occurs; (b) Contact geometry on *xy* plane.

In Figure 11, point *d* represents the contact point on the contact strip surface which is geometrically determined by assuming that the normal contact force, $\mathbf{f}_n$, and its corresponding pseudo penetration are perpendicular to both the flat surface of the contact strip and the contact wire cylindrical contact surface. As point *c* is collinear with *a* and *b*, its coordinate position is obtained as:

$$\begin{aligned} \mathbf{r}_d &= \mathbf{r}_a + \lambda_{ad}\hat{\mathbf{u}}_{ab} \\ \lambda_{ad} &= \hat{\mathbf{u}}_{ab} \cdot \mathbf{r}_{ac} = \hat{\mathbf{u}}_{ab} \cdot (\mathbf{r}_c - \mathbf{r}_a) \end{aligned} \tag{18}$$

such that λ_{ad} is the length between point *a* and *d* which can be retrieved as the scalar projection between the versor $\hat{\mathbf{u}}_{ab}$ and vector $\mathbf{r}_{ac}$ that goes from point *a* to *c*:

$$\lambda_{ad} = \hat{\mathbf{u}}_{ab}^T \mathbf{r}_{ac} = \hat{\mathbf{u}}_{ab}^T (\mathbf{r}_c - \mathbf{r}_a) \tag{19}$$

With the contact geometry established, the normal contact force, f_n, is obtained by using a purely elastic Hertzian normal contact force model, written as:

$$f_n = \begin{cases} K\delta & , \ \delta > 0 \\ 0 & , \ \delta \le 0 \end{cases} \tag{20}$$

where K is the contact stiffness , $\delta = \left\| \mathbf{r}_c - \mathbf{r}_d \right\| - r_{cw}$ is the pseudo normal penetration and r_{cw} is the contact wire radius. In this work the contact stiffness used is 200×10^3 N/m following the recommendations for key parameters on pantograph-catenary numerical

models established in PantoTRAIN European project [54].

As the contact surface of the contact wire is concentric with its cross section centre, the normal contact force is directly applied in point *c*, being the equivalent contact forces and moments, $\mathbf{f}_i^c$ and $\mathbf{f}_j^c$, applied at nodes *i* and *j* of the contact wire finite element, evaluated as:

$$\begin{bmatrix} \mathbf{f}_i^c \\ \mathbf{f}_j^c \end{bmatrix} = \mathbf{N}(\xi)^T f_n \hat{\mathbf{u}}_{dc} \tag{21}$$

On the contact strip the normal force is applied on point *d* such that the resultant force and transport moment, $\mathbf{f}_3^c$ and $\mathbf{n}_3^c$, to be applied on the lumped mass pantograph top body mass centre are evaluated as:

$$\begin{aligned} \mathbf{f}_3^c &= f_n \hat{\mathbf{u}}_{cd} \\ \mathbf{n}_3^c &= \tilde{\mathbf{s}}_d'^3 \, \mathbf{A}_3^T \mathbf{f}_3^c \end{aligned} \tag{22}$$

where $\mathbf{s}_d'^3$ is the position of point *d* relative to the top body local reference frame $(\xi, \eta, \zeta)_3$.

5.2 Pantograph-Catenary Co-Simulation

The catenary is modelled with a finite element formulation being a dynamic linear system integrated with a Newmark family numerical integrator set implicitly with fixed time step [59]. The multibody pantograph model nonlinear dynamics is evaluated as a forward dynamics problem being its solution obtained with a variable time step and variable order numerical integrator of the Gear type [60]. In the co-simulation procedure implemented here, each sub-system performs its dynamic evaluation independently from the other. In order that each sub-system can proceed with its integration procedure the state variables of each subsystem are shared. Since the contact evaluation needs to access the deformed finite element mesh of the catenary to search for contact along the catenary wire, the contact is evaluated on the finite element dynamic solver, on the catenary side. To this effect, as depicted in Figure 13, the state variables supplied by the multibody code in which the pantograph is defined, are the position of the contact strip extremities, $\mathbf{r}_a$ and $\mathbf{r}_b$. With these coordinates, the catenary subsystem evaluates the contact and returns, as its state variables, the resulting contact force vector, $\mathbf{f}_c$, and its point of application $\mathbf{r}_c$ on the collector strip.

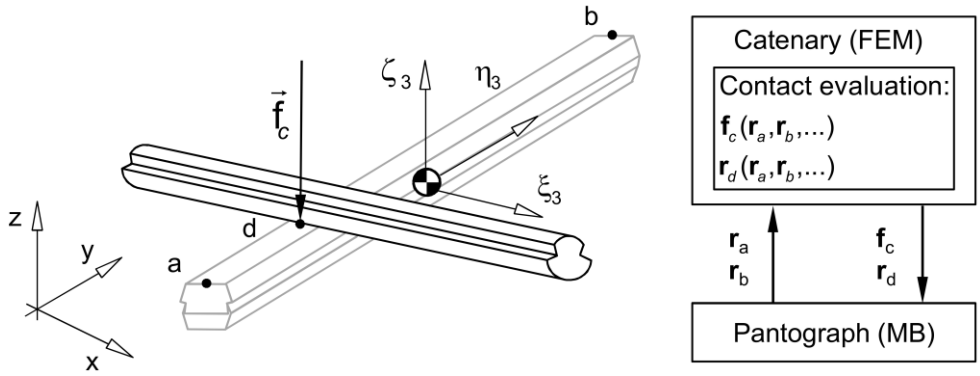

Figure 13: State variable exchange between catenary and pantograph subsystems.

The compatibility between the heterogeneous integration procedures imposes that the state variables, or a reliable prediction, are readily available at each evaluate time step. This is guaranteed by a state variable time interpolation/extrapolation scheme presented in Figure 14. The accuracy and stability of this procedure relies on the integration step used on both systems and in ensuring that the maximum time step size of the multibody pantograph sub-system never exceeds the catenary fixed time step [35,61].

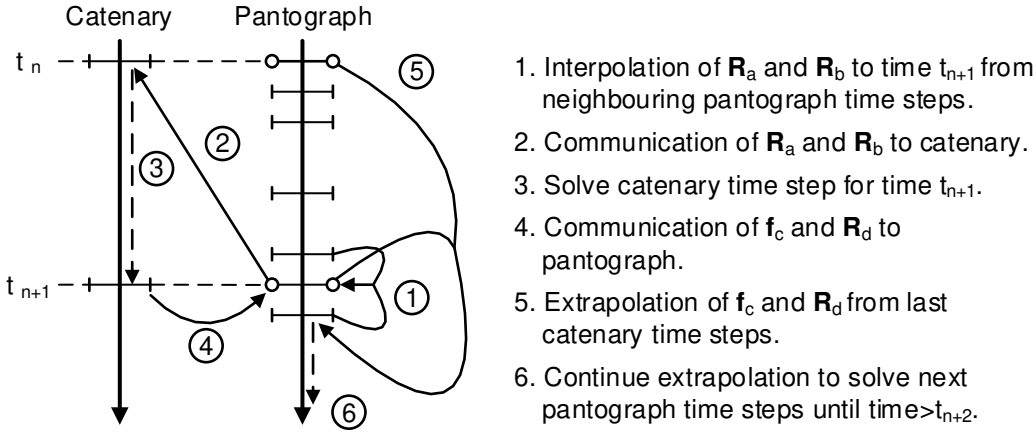

Figure 14: Sate variable time interpolation/extrapolation in pantograph-catenary co-simulation.

6 Case Studies

To demonstrate the approach proposed here to handle the pantograph-catenary dynamics for general geometry railway tracks, two case scenarios are considered. One is a realistic case where the catenary complete layout and track geometry are obtained through the project data of a catenary line that is currently in operation. The second case is an exercise following the insertion of a catenary model in tracks with different curvature. In both cases the pantograph-catenary contact quality is evaluated through the statistical analysis of the developed contact forces filtered at 0-20 Hz, following the standards EN50367 and EN50119. Also, as both catenary systems used here are designed for high speed operation,

all the simulations consider a vehicle speed of 300 km/h, where the pantograph uplift force is tuned for a mean contact force of 157.3 N on a straight track.

6.1 Existing Catenary Network

Since the procedure presented here is able to cope with any generalised trajectory of the track, the first case study concerns a realistic catenary associated to the track geometry, described in Figure 15. The catenary layout and specifications are taken directly from the technical plans of a catenary system in current operation. The pantograph model is that of the overhead equipment commonly used for high speed trains in operation on the track.

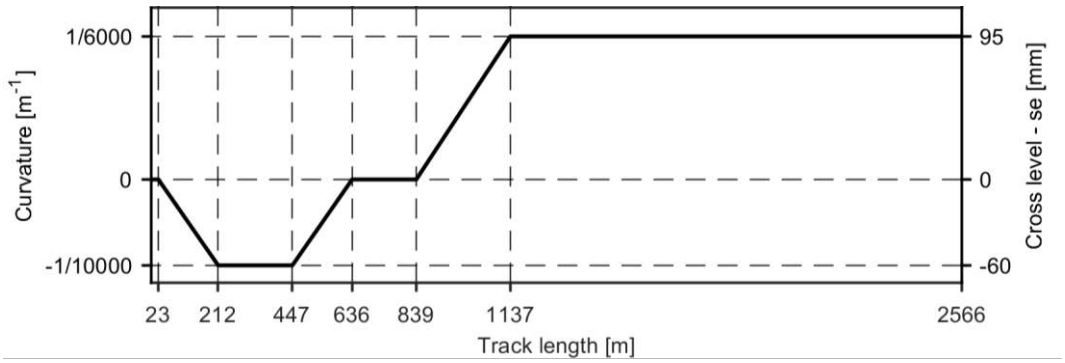

Figure 15: Track geometry considered on the realistic case.

Both the general catenary design characteristics and pantograph lumped mass parameters are presented in Table 2. The technical designs establish no pre-sag in this catenary system and for the track interval considered here a constant alternating stagger of (+200,-200) mm is specified.

Catenary		Pantograph	
Contact wire tension [N]	20000	m1 [kg]	5.58
Messenger wire tension [N]	16250	m2 [kg]	8.78
Contact wire height [m]	5.3	m3 [kg]	7.75
Encumbrance [m]	1.25	k1 [N/m]	178.45
Stagger [mm]	(+200,-200)	k2 [N/m]	15487.00
Span lengths [m]	60-52	k3 [N/m]	7000.00
Damping α [1/s]	0.0125	c1 [Ns/m]	108.39
Damping β [s]	0.0001	c2 [Ns/m]	0.09
Vehicle roof top height [m]	4.05	c3 [Ns/m]	45.85

Table 2: Catenary and pantograph model specifications.

The track geometry is characterised by two curves, with a straight segment in between, where two catenary sections are defined. A representation of the resulting catenary finite element mesh of the catenary system, after being statically loaded, is presented in Figure 16.

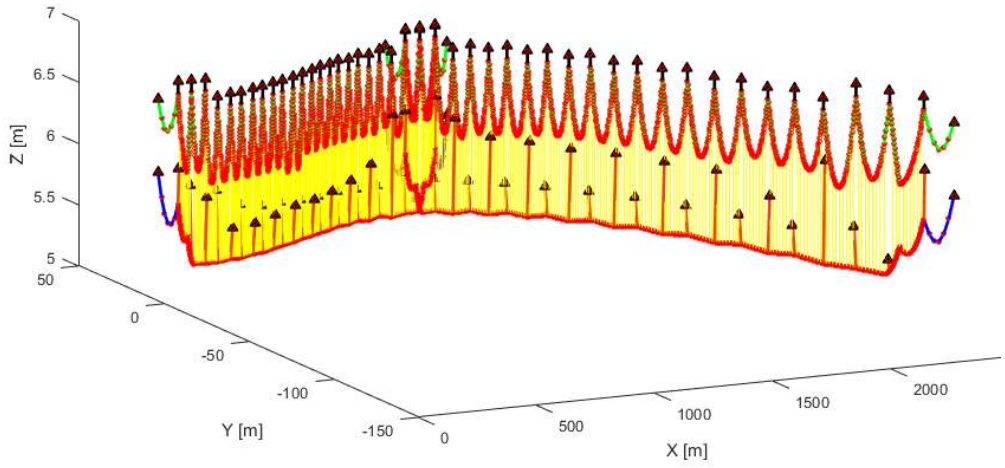

Figure 16: Representation of the deformed finite element catenary mesh for different.

Two regions of interest are selected for the analysis of the catenary: one on the straight section of the track; and other on the curved section with a 6000 m radius track, being an interval containing 2 spans considered. The contact quality parameters associated to the contact forces and the steady arm uplifts are presented in Table 3.

Track	Straight	R6000	Limit Values
Track Interval [m]	642-757	1833-1945	
Force maximum [N]	253.1	275.5	350
Force minimum [N]	80.2	90.0	-
Force amplitude [N]	172.9	185.6	-
Force mean [N]	157.3	156.9	157.3
Force standard deviation [N]	30.4	34.7	47.1
Force statistical minimum [N]	66.1	52.8	-
Steady arm uplift (642m,1833m) [m]	0.079	0.081	0.16
Steady arm uplift (702m,1889m) [m]	0.079	0.070	0.16
Steady arm uplift (757m,1945m) [m]	0.075	0.081	0.16

Table 3: Contact force statistics for the contact quality evaluation considering force and steady arm uplift.

Although the results cannot be directly compared since the spans have all different lengths, it can be observed that a marginal contact quality degradation occurs on the curved section. This is noted by the slightly higher standard deviation and contact force maximum. Nevertheless, all parameters are under their allowable limits. Moreover, by observing the contact forces developed along the track, presented in Figure 17, on the curved track it is possible to notice an alternating difference on the maximum peaks. These are found slightly before the pantograph passage over the cantilever supports and its effects can be related to the differences found on the steady arm uplifts. Note also that the higher maximum peaks coincide with the lateral offsets located in the inner side of the curved track.

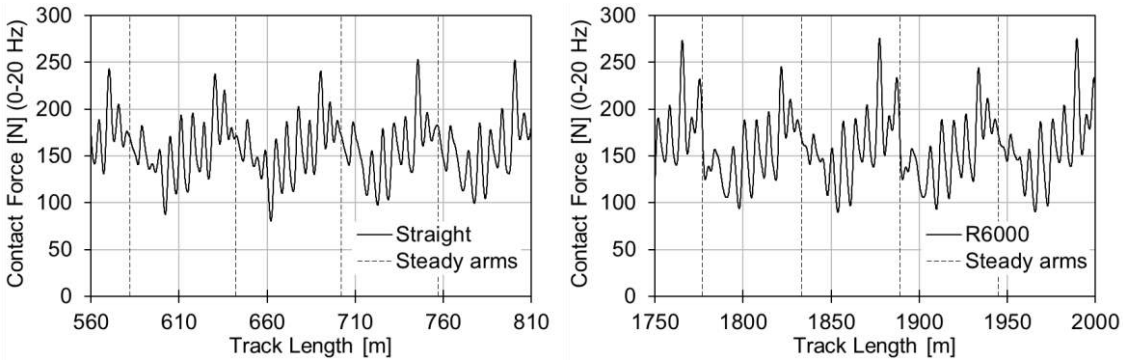

Figure 17: Contact force evaluated along the track length.

6.2 Curve Insertion Case

The catenary and pantograph models chosen for this application case are the models presented on the pantograph catenary benchmark [24]. Their main specifications are presented in Table 4.

Catenary		Pantograph	
Contact wire tension [N]	22000	m1 [kg]	6
Messenger wire tension [N]	16000	m2 [kg]	9
Contact wire height [m]	5.3	m3 [kg]	7.5
Encumbrance [m]	1.2	k1 [N/m]	160
Stagger [mm]	(+200,-200)	k2 [N/m]	15500
Span lengths [m]	55	k3 [N/m]	7000
Damping α [1/s]	0.0125	c1 [Ns/m]	100
damping β [s]	0.0001	c2 [Ns/m]	0.1
Vehicle roof top height [m]	4.05	c3 [Ns/m]	45

Table 4: Benchmark catenary and pantograph model specifications.

Three different track geometries are considered to insert the catenary model: a straight line; and, two scenarios that start as a straight track and transition to respectively a curved track with a 6000 m and 4000 m and a cross level of 110 mm and 160 mm. Each catenary as a total of 22 spans, being the starting straight portion on the curved tracks composed by 4 spans, followed by 5 spans of transition. Although the track with a 4000 m curve radius is a tight curve for the operating speed considered, all the track geometries here are compliant with the European standard EN13803-1. Four catenary system setups with different staggers are considered. Three setups have an alternating stagger of (+200,-200) mm and are set along each of the specified track paths. In the fourth setup, a stagger of (+200,0) mm on the curved portion of the 4000 m radius curved track is considered. A representation of the resulting catenary finite element meshes, after being statically loaded, is presented in Figure 18.

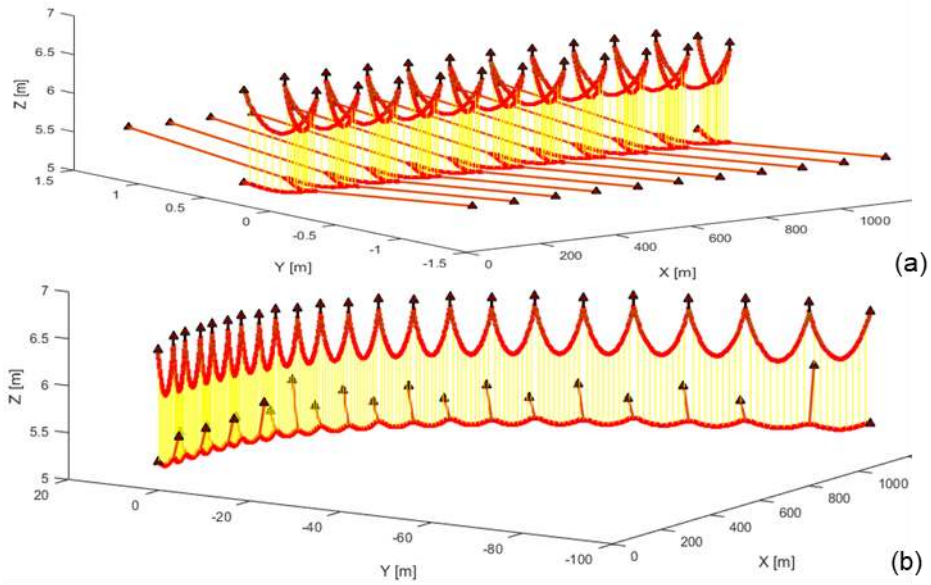

Figure 18: Representation of the deformed finite element catenary mesh for different staggers: a) Straight track (+200,-200) mm , b) Track with 4000m curve (+200,0) mm.

The statistical parameters resulting from the contact force evaluation on each of the catenary systems and the steady arm uplifts are presented in Table 5. The region of interest set for the analyses [660m-770m] contains two spans where its centre cantilever corresponds to the imposed offset on the inner side of the curve. Comparing the results obtained between the straight catenary and the catenary inserted in the largest radius curved track, only marginal differences can be found. However, these show a slight tendency to contact quality degradation, which becomes clear when observing the results for the smaller radius curved track with the same stagger. Here, although the mean contact force remains close to its target, both the maximum force and standard deviation increase exceeding the standard limits. The negative force statistical minimum is indicative of probability of loss of contact, which is verified in the unfiltered results with a percentage of loss of contact of 4%.

Track	Straight	R6000	R4000	R4000	Limit Values
Stagger [mm]	(+200,-200)	(+200,-200)	(+200,-200)	(+200,0)	
Force maximum [N]	254.3	252.8	425.1	243.9	350
Force minimum [N]	90.7	94.1	29.5	88.4	-
Force amplitude [N]	163.6	158.7	395.7	155.5	-
Force mean [N]	157.3	156.8	156.6	156.0	157.3
Force standard deviation [N]	40.3	40.8	62.1	38.0	47.1
Force statistical minimum [N]	278.3	279.3	343.0	270.1	-
Steady arm uplift (660m) [m]	0.047	0.049	0.063	0.047	0.16
Steady arm uplift (715m) [m]	0.047	0.049	0.033	0.053	0.16
Steady arm uplift (770m) [m]	0.047	0.050	0.062	0.049	0.16

Table 5: Contact force statistical evaluation and steady arm uplifts.

When changing the staggering to (+200,0) mm in the 4000 m radius curved track, the contact quality is greatly improved returning to nominal operating levels. The evolution of the contact forces along the track is presented in Figure 19 for the different scenarios. The maximum force peaks are observed near the pantograph passage under the cantilevers in correspondence with the steady arm uplift results.

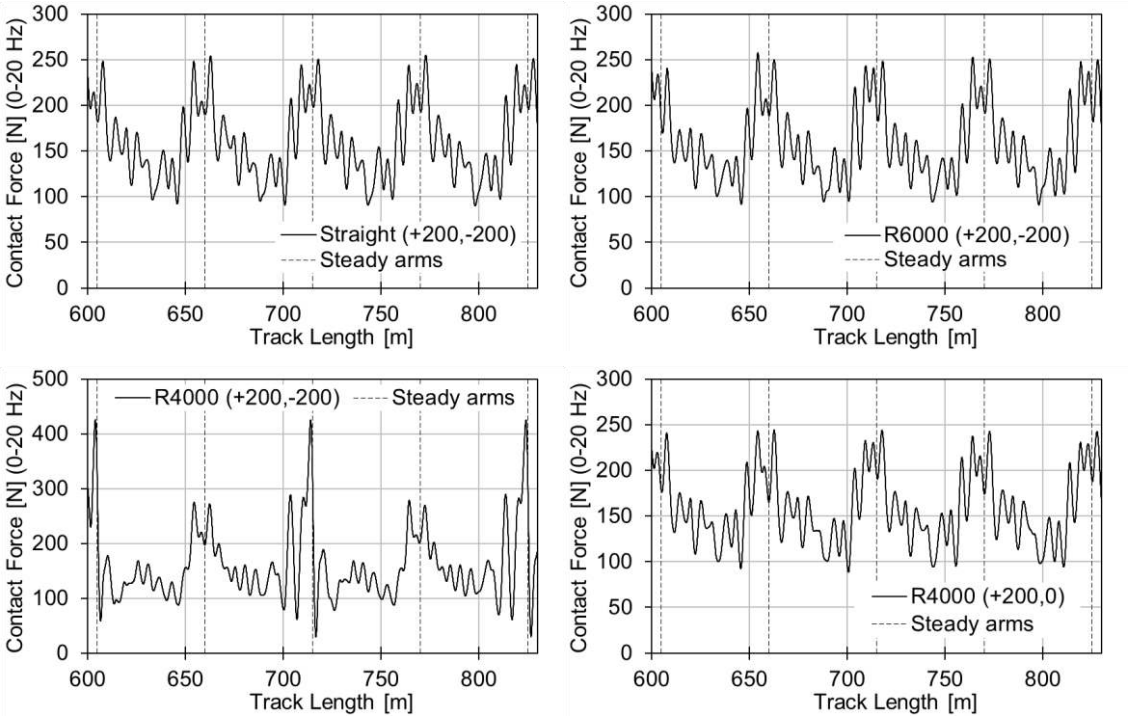

Figure 19: Contact force evaluated along the track length.

In the catenary associated to the curved track with 4000 m radius and a (+200,-200) mm stagger it is possible to distinguish force peaks according the offset imposed on each support. The higher force peaks correspond to the offset imposed on the inner side of the curve. These stiff spots are due to the orientation of the steady arm which is controlled by the forces due to the contact wire, as represented in Figure 20. The steady arm orientation is defined by its resulting angle, θ, with the horizontal plane. The force on the steady arm, $\mathbf{f}_r$, can be decomposed in a lateral force component associated to the imposed contact wire stagger, $\mathbf{f}_{lat}$, and a vertical force component, $\mathbf{f}_z$, that supports a residual part of the contact wire weight and set is vertical position correctly.

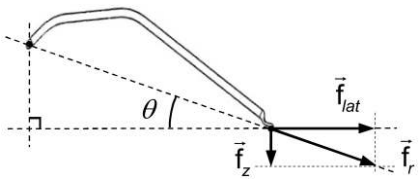

Figure 20: Contact wire force solicitations at the steady arm.

The vertical force component does not change greatly from pole to pole being the orientation of the steady arm mainly dictated by the lateral forces which in turn depend on the imposed offsets at each cantilever. Figure 21, shows the lateral forces developed at each cantilever and the resulting steady arm orientation angle for each of the cases considered here. The positive lateral forces refer to the forces acting away from the pole being negative when acting towards the pole defining the cantilever pull-off or push-off configuration. Notice that these lateral forces remain constant on the straight catenary but in the curved tracks present an offset from pole to pole. It is also possible to observe how this offset develops on the curve transition. The small lateral forces on the inner side of the curved track with 4000 m radius and a (+200,-200) mm stagger are very low which results in an excessive rotation angle of the steady arm of about 62°. Consequently, this originates a critical stiff spot for the pantograph passage, which turns to be the main cause for the observed degradation of the contact quality. This is in agreement with the requisites described in [43] which establish a minimal lateral force of 80N and a maximum angle of the steady arm of 20°. By changing the staggering to (+200,0) mm these requisites are fulfilled and the contact quality is improved. Also notice that in the curved portion of the track, the lateral forces become positive on all the poles meaning that all the cantilevers are to be set in a pull-off configuration, as it can be observed by the steady arm orientations represented in Figure 18 (b).

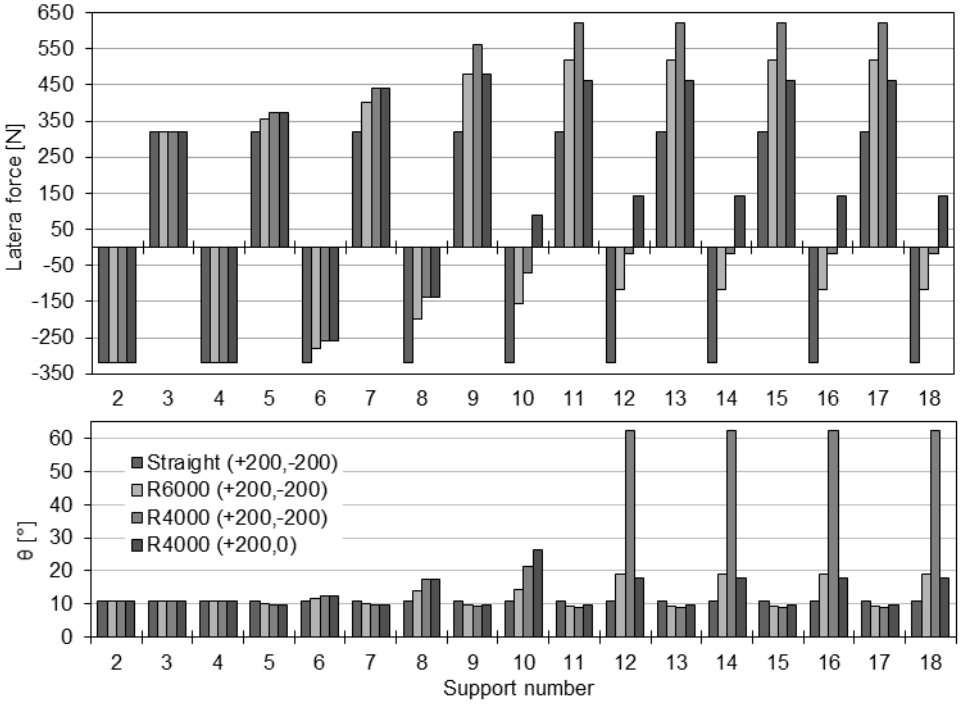

Figure 21: Lateral forces and resulting steady arm angle at each cantilever support.

7 Conclusions

A novel numerical procedure for the dynamic analysis of pantograph–catenary interaction on generalized track trajectories is presented here. The geometric description of the track running surface by a moving local frame of reference is the basis to build the catenary finite element model and to describe the general path of the pantograph. Two demonstration cases are presented, one represents an existing scenario where both the catenary layout and track geometry are obtained from the technical designs of a current track in operation. The other case study presents a variation on the benchmark study of pantograph–catenary interaction by defining it in tracks with different curve radius and contact wire staggering. It is shown that for large curve radius tracks the contact quality is marginally affected by the curvature. For smaller radius curves, the staggering design plays a fundamental role in maintaining the contact quality.

The first main contribution of the numerical tool presented here is the possibility to analyse more realistic catenary systems which are modelled using track and catenary design data of already constructed or projected railway lines, not being limited to straight tracks. It also provides a methodology to study the pantograph–catenary dynamics over curved tracks including the influence of the staggering design. Moreover, this approach opens the possibility to analyse novel case studies of interest to the rail industry. One is the influence of wind loads on the pantograph-catenary contact quality in curved tracks, where the wind solicitations imply a change on the lateral forces imposed by the contact wire at its cantilever support. There are also cases where optimisation procedures in conjunction with pantograph-catenary dynamic analysis applications can be used to reach optimised designs of pantograph or catenary systems. In such cases, considering the optimisation only in straight tracks might be limitative when contemplating a generalised track path. One other aspect of interest is the analysis of pantograph-catenary interaction over tracks with small radius curves, particularly on railway tracks that are to be upgraded for higher operational speeds, which often require a change on the contact and messenger wire axial tension, as well as the catenary layout geometry.

Acknowledgements

The work reported here has been developed in collaboration with Politecnico di Milano and funded by the Portuguese Foundation of Science and Technology (FCT) PhD program, SFRH/BD/88515/2012. Also, this work was supported by FCT, through

IDMEC, under LAETA, project UID/EMS/50022/2019. The authors want to thank Prof. Stefano Bruni for accepting and promoting this collaboration which was essential to develop this work.

References

[1] Shing AWC, Wong PPL. Wear of pantograph collector strips. J. Rail Mass Transit. 2008;222:169–176.
[2] ERRAC. Strategic Rail Research Agenda 2020. Brussels, Belgium; 2007.
[3] EC - European Commission. Roadmap to a Single European Transport Area - Towards a Competitive and Resource Efficient Transport System. Brussels, Belgium, Belgium; 2011.
[4] Poetsch G, Evans J, Maisinger R, et al. Pantograph/Catenary Interaction and Control. Veh. Syst. Dyn. 1997;28:159–195.
[5] Ikeda K. Optimization of Overhead Contact Lines for Shinkansen Speed Increases. JR EAST Tech. Rev. 12th ed. 2008;64–69.
[6] Pombo J, Antunes P. A Comparative Study Between Two Pantographs In Multiple Pantograph High-Speed Operations. Internatinal J. Railw. Technol. 2013;2:83–108.
[7] Liu Z, Jönsson PA, Stichel S, et al. Implications of the operation of multiple pantographs on the soft catenary systems in Sweden. Proc. Inst. Mech. Eng. Part F J. Rail Rapid Transit. 2016;230:971–983.
[8] Bucca G, Carnevale M, Collina A, et al. Adoption of different pantographs preloads to improve multiple collection and speed up existing lines. Veh. Syst. Dyn. 2012;50:403–418.
[9] Antunes P, Ambrósio J, Pombo J, et al. Dynamic Analysis of the Pantograph-Catenary Interaction on Overlap Sections for High-Speed Railway Operations. Proc. Second Int. Conf. Railw. Technol. Res. Dev. Maint. Stirlingshire, UK: Civil-Comp Press; 2014.
[10] Harèll P, Drugge L, Reijm M. Study of Critical Sections in Catenary Systems During Multiple Pantograph Operation. Proc. Inst. Mech. Eng. Part F J. Rail Rapid Transit. 2005;219:203–211.
[11] Mei G, Zhang W, Zhao H, et al. A hybrid method to simulate the interaction of pantograph and catenary on overlap span. Veh. Syst. Dyn. 2006;44:571–580.
[12] Ambrósio J, Pombo J, Pereira M, et al. Optimization of high-speed railway pantographs for improving pantograph-catenary contact. Theor. Appl. Mech. Lett. 2013;3.
[13] Gregori S, Tur M, Nadal E, et al. An approach to geometric optimisation of railway catenaries. Veh. Syst. Dyn. 2017;3114:1–25.
[14] Bruni S, Bucca G, Collina A, et al. Numerical and Hardware-In-the-Loop Tools for the Design of Very High Speed Pantograph-Catenary Systems. J. Comput. Nonlinear Dyn. 2012;7:041013.
[15] Van OV, Massat JP, Laurent C, et al. Introduction of variability into pantograph-catenary dynamic simulations. Veh. Syst. Dyn. 2014;52:1254–1269.
[16] Carnicero A, Jimenez-Octavio JR, Sanchez-Rebollo C, et al. Influence of Track Irregularities in the Catenary-Pantograph Dynamic Interaction. J. Comput. Nonlinear Dyn. 2012;7:041015.
[17] Pombo J, Ambrósio J, Pereira M, et al. Influence of the Aerodynamic Forces on the Pantograph-Catenary System for High Speed Trains. Veh. Syst. Dyn. 2009;47:1327–1347.
[18] Kulkarni S, Pappalardo CM, Shabana AA. Pantograph/Catenary Contact Formulations. J. Vib. Acoust. 2016;139:011010.
[19] Song Y, Liu Z, Wang H, et al. Nonlinear analysis of wind-induced vibration of high-speed railway catenary and its influence on pantograph–catenary interaction. Veh. Syst. Dyn. 2016;54:723–747.
[20] Facchinetti A, Bruni S. Hardware-in-the-loop hybrid simulation of pantograph–catenary interaction. J. Sound Vib. 2012;331:2783–2797.
[21] Schirrer A, Aschauer G, Talic E, et al. Catenary emulation for hardware-in-the-loop pantograph testing with a model predictive energy-conserving control algorithm. Mechatronics. 2017;41:17–28.
[22] Ambrósio J, Antunes P, Pombo J, et al. A Computational Procedure for the Dynamic Analysis of the Catenary-Pantograph Interaction in High-Speed Trains. J. Theor. Appl. Mech. 2012;50:681–699.
[23] Nåvik P, Rønnquist A, Stichel S. Identification of system damping in railway catenary wire systems from full-scale measurements. Eng. Struct. 2016;113:71–78.
[24] Bruni S, Ambrosio J, Carnicero A, et al. The results of the pantograph–catenary interaction

benchmark. Veh. Syst. Dyn. 2014;53:412–435.
[25] Facchinetti A, Bruni S. Special issue on the pantograph–catenary interaction benchmark. Veh. Syst. Dyn. 2015;53:303–304.
[26] Teichelmann G, Schaub M, Simeon B. Modelling and simulation of railway cable systems. ZAMM Zeitschrift fur Angew. Math. und Mech. 2005;85:864–877.
[27] Ambrósio J, Pombo J, Antunes P, et al. PantoCat statement of method. Veh. Syst. Dyn. 2015;53:314–328.
[28] Tur M, García E, Baeza L, et al. A 3D absolute nodal coordinate finite element model to compute the initial configuration of a railway catenary. Eng. Struct. 2014;71:234–243.
[29] Rønnquist A, Nåvik P. Dynamic assessment of existing soft catenary systems using modal analysis to explore higher train velocities: A case study of a Norwegian contact line system. Veh. Syst. Dyn. 2015;53:756–774.
[30] Nåvik P, Rønnquist A, Stichel S. Variation in predicting pantograph–catenary interaction contact forces, numerical simulations and field measurements. Veh. Syst. Dyn. 2017;55:1265–1282.
[31] Ambrósio J, Pombo J, Pereira M, et al. Recent Developments in Pantograph-Catenary Interaction Modelling and Analysis. Int. J. Railw. Technol. 2012;1:249–278.
[32] Nikravesh PE. Computer-Aided Analysis of Mechanical Systems. Englewood Cliffs, New Jersey: Prentice-Hall; 1988.
[33] Ambrósio J, Antunes P, Pombo J. On the Requirements of Interpolating Polynomials for Path Motion Constraints. In: Kecskeméthy A, Geu Flores F, editors. Mech. Mach. Sci. Springer International Publishing; 2015. p. 179–197.
[34] Pombo J, Ambrósio J. General Spatial Curve Joint for Rail Guided Vehicles: Kinematics and Dynamics. Multibody Syst. Dyn. 2003;9:237–264.
[35] Ambrósio J, Pombo J, Rauter F, et al. A Memory Based Communication in the Co-Simulation of Multibody and Finite Element Codes for Pantograph-Catenary Interaction Simulation. In: Bottasso C.L. E, editor. Multibody Dyn. Dordrecht, The Netherlands: Springer; 2008. p. 211–231.
[36] Esveld C. Modern Railway Track. Duisburg, Germany: MRT-Productions; 1989.
[37] Yamaguchi F. Curves and Surfaces in Computer Aided Geometric Design. Springer-Verlag; 1988.
[38] Mortenson ME. Geometric Modeling. New York, New York: Wiley; 1985.
[39] Iverson W. Analysis of the Reconstruction of Rail Geometry from Curvature Data. IEEE Trans. Ind. Appl. 1974. p. 368–379.
[40] Pombo J, Ambrósio J. Modelling Tracks for Roller Coaster Dynamics. Int. J. Veh. Des. 2007;45:470–500.
[41] Przemieniecki JS. Theory of Matrix Structural Analysis. New York: McGraw-Hill; 1968.
[42] UIC 606-1 OR standart. Consequences of the application of the kinematic gauges defined by UIC leaflets in the 500 series on the design of the contact lines. UIC; 1987.
[43] Friedrich K, Puschmann R, Schmieder A, et al. Contact Lines for Electric Railways: Planning, Design, Implementation, Maintenance. 3rd ed. Publicis; 2018.
[44] TSI ENE. Technical specifications for interoperability relating to the ‘energy’ subsystem of the rail system in the Union. Official Journal of the European Union. 1301/2014/EU; 2014.
[45] ERA - European Rail Agency. Study on Interface EURO/1950 pantographs and OCL design - ERA/2013/INTEROP/OP/01. European Union; 2013.
[46] Rayleigh JWS. The Theory of Sound, Volume One. 2nd ed. Dover Publications; 2013.
[47] Arora JS. Introduction to Optimum Design. 3ed. Boston: Academic Press; 2012.
[48] EN 15273-1: Railway applications - Gauges - Part 1: General - Common rules for infrastructure and rolling stock. Brussels, Belgium: CENELEC; 2013.
[49] Pombo J, Ambrósio J. Influence of pantograph suspension characteristics on the contact quality with the catenary for high speed trains. Comput. Struct. 2012;110–111:32–42.
[50] Flores P. Kinematics and dynamics of multibody systems with imperfect joints : models and case studies. Lect. notes Appl. Comput. Mech. Berlin: Springer; 2008.
[51] Ambrósio J, Verissimo P. Improved Bushing Models for General Multibody Systems and Vehicle Dynamics. Multibody Syst. Dyn. 2009;22:341–365.
[52] Collina A, Bruni S. Numerical Simulation of Pantograph-Overhead Equipment Interaction. Veh. Syst. Dyn. 2002;38:261–291.
[53] Vyasarayani CP, Uchida T, Carvalho A, et al. Parameter identification in dynamic systems using the homotopy optimization approach. Multibody Syst. Dyn. 2011;26:411–424.
[54] Ambrósio J, Pombo J, Facchinetti A, et al. Key Parameters for Pantograph/Catenary Numerical Models - PantoTRAIN Technical Report D1.1. Brussels, Belgium: UNIFE; 2010.
[55] Pombo J, Ambrosio J. Environmental and track perturbations on multiple pantograph interaction

with catenaries in high-speed trains. Comput. Struct. 2013;124:88–101.
[56] Wang J, Ma Z, Hulbert GM. A Gluing Algorithm for Distributed Simulation of Multibody Systems. Nonlinear Dyn. 2003;34:159–188.
[57] Schweizer B, Li P, Lu D. Explicit and Implicit Cosimulation Methods: Stability and Convergence Analysis for Different Solver Coupling Approaches. J. Comput. Nonlinear Dyn. 2015;10:051007.
[58] Toridis TG, Khozeimeh K. Computer analysis of rigid frames. Comput. Struct. 1971;1:193–221.
[59] Bathe K-J. Finite element procedures in engineering analysis. Prentice-Hall Civ. Eng. Eng. Mech. Ser. Englewood Cliffs, N.J.: Prentice-Hall; 1982.
[60] Gear CW. Simultaneous Numerical Solution of Differential-Algebraic Equations. IEEE Trans. Circuit Theory. 1971;18:89–95.
[61] Rauter FG, Pombo J, Ambrósio J, et al. Contact Model for The Pantograph-Catenary Interaction. J. Syst. Des. Dyn. 2007;1:447–457.